New Solutions for Slow Moving Kinks in a Forced Frenkel-Kontorova Chain

Phoebus Rosakis and Anna Vainchtein

New Solutions for Slow Moving Kinks in a Forced Frenkel-Kontorova Chain

Phoebus Rosakis
Department of Applied Mathematics
University of Crete
Heraklion 71409, Greece
rosakis@tem.uoc.gr

Anna Vainchtein
Department of Mathematics
University of Pittsburgh
Pittsburgh, PA 15260, USA
aav4@pitt.edu

May 15, 2012

Abstract

We construct new traveling wave solutions of moving kink type for a modified, driven, dynamic Frenkel-Kontorova model, representing dislocation motion under stress. Formal solutions known so far are inadmissible for velocities below a threshold value. The new solutions fill the gap left by this loss of admissibility. Analytical and numerical evidence is presented for their existence; however, dynamic simulations suggest that they are probably unstable.

1 Introduction

The first study of dislocation motion through a discrete model was performed by Atkinson and Cabrera [1], followed by Celli and Flytzanis [4] and Ishioka [8]. Atkinson and Cabrera [1] utilize a variant of the discrete sine-Gordon equation, which arises in the dynamic version of the Frenkel-Kontorova model. They seek traveling wave solutions corresponding to uniformly moving dislocations under applied stress, represented by a constant forcing term. To the present day, analytical progress on the forced problem has been limited, while some numerical conclusions have been drawn by Peyrard and Kruskal [11]. In [1], the trigonometric potential of the Frenkel-Kontorova model, responsible for the nonlinearity in the sine-Gordon equation, is replaced by a piecewise smooth potential with quadratic wells. A similar choice is made in [4, 8]. The resulting equation for traveling waves reduces to a linear one, provided the solution satisfies an *admissibility condition*. This requires that to the right of a single transition point (the dislocation core), the solution

take values entirely in one of two quadratic valleys of the potential, and in the other valley to the left. Solutions of the reduced linear equation are found semi-analytically. Traveling waves are found to exist only if the stress and speed satisfy an algebraic relation, the *kinetic relation* of the dislocation. A remarkable prediction of this relation was that dislocations exceed the speed of shear waves at sufficiently high stress. This was recently confirmed experimentally [10]. Another feature is the presence of multiple singularities and discontinuities in the graph of stress versus velocity, located at a sequence of special resonance velocities that accumulate at zero; see Fig. 1. However, as emphasized by Earmme and Weiner [5] (see also [9]), below a threshold velocity, solutions of the linear problem violate the admissibility condition; this issue was not fully recognized in [1]. This rules out solutions in the entire interval containing singularities as inadmissible, since all resonance velocities are below the threshold velocity.

The problem of existence of traveling waves at velocities below the threshold value has remained open to the best of our knowledge; this also applies to the results of [4]. This is the main issue addressed in the present paper.

We present compelling analytical and numerical evidence that for velocities below the threshold value, there is a new type of traveling wave solution $u(\xi)$, $\xi = x - Vt$, which actually *violates* the usual admissibility conditions (but satisfies a suitable generalization). The model employs a piecewise smooth two well potential $\Phi(u)$ with two quadratic branches meeting at the *spinodal value* $u = 0$. The usual admissibility conditions require that the solution vanish (go through the spinodal value) at precisely one point, say $\xi = 0$, where it transitions between the two quadratic valleys of Φ, so that it must be strictly monotone in the neighborhood of the transition point. Instead, the new solutions we find are equal to zero on an entire finite interval, and lie in different potential valleys on either side of this interval.

The motivation for considering such solutions comes from a more elaborate model [15] where $\Phi(u)$ is piecewise quadratic but continuously differentiable. Its graph consists of three parabolas, two convex ones separated by a concave one, defined on the *spinodal range* of u values. Any kink solution $u(\xi)$ that transitions between the two convex potential valleys must therefore take values in the spinodal range for ξ in some interval, say $[-z, z]$. Here $z > 0$ is an unknown of the problem and is found to depend on the size of the spinodal range. Now $\Phi'(u)$ is trilinear with two increasing branches and a decreasing one between them. When the slope of the latter is treated as a parameter and approaches $-\infty$, so that the spinodal range tends to degenerate to the point $u = 0$, a surprising observation is made in [15]: The interval $-z \le \xi \le z$ where $u(\xi)$ takes values in the spinodal range does not shrink to a point, as one might expect. Rather, z approaches a positive value in the limit. The limiting potential is the piecewise smooth biquadratic one considered in [1, 4, 8] where admissible low-velocity kinks have not been found so far. It is thus natural to directly try the new type of solutions mentioned in the previous paragraph, that vanish

(equal the degenerate spinodal value) over an interval $[-z, z]$, where $z > 0$, in the context of the Atkinson-Cabrera problem.

While we do not rigorously prove their existence, we are able to construct the new solutions semi-analytically; we present approximate analytical and also numerical evidence of their existence. We find that they bifurcate from the classical Atkinson-Cabrera solutions, at precisely the threshold velocity V_0 below which the latter become inadmissible. The new solutions exist essentially over the entire velocity range $0 < V < V_0$; thus they seem to close the entire gap left by loss of admissibility of the Atkinson-Cabrera solutions.

The kinetic relation between the applied stress σ (constant forcing term) and velocity V of moving kinks (dislocations) described by the new solutions is entirely different from the (inadmissible) one obtained in [1] over the velocity range $0 < V < V_0$; see Fig. 5 where the two are compared. Unfortunately, its physical significance is in question, since the new solutions appear to be unstable. This is suggested by numerical simulations of the Frenkel-Kontorova chain dynamics, where kinks either stop or move with velocities above V_0. Recently a similar trend was observed in experiments that measured kinetic relations for dislocations in actual two dimensional plasma crystals [10]. Our results are consistent with the findings of [15], where slow kinks are apparently unstable when the spinodal range is sufficiently narrow. In contrast, *some* slow kinks do become stable if the spinodal range is sufficiently wide in [15], as is also observed in [5, 11].

The paper is organized as follows. In Section 2 we recall the dynamical driven Frenkel-Kontorova model and the equation for traveling wave solutions that describes steady motion of a moving dislocation, or kink, under stress. We consider the case of a piecewise quadratic potential and recall the main properties of the explicit Atkinson-Cabrera solution. The loss of admissibility of this solution in the low-velocity regime motivates us to relax the strict monotonicity assumption made in [1]. We derive in Section 3 conditions for a new type of kink solutions. These conditions include a linear integral equation of the first kind, whose kernel is related to the formal Atkinson-Cabrera solution, regardless of the admissibility of the latter. Solving the integral equation yields a shape function that can be used to obtain the new kink solution. The support $[-z, z]$ of the shape function, which depends on the velocity of the moving kink, is the interval where the new kink solutions take the spinodal value. In Section 4 we use linear and quadratic approximations of the kernel in the integral equation to obtain approximations of the shape function under the assumption that z is small. It turns out that the shape function is a distribution that involves two delta functions concentrated at $\pm z$. In contrast, the shape functions obtained in [15] are bounded. Our results show that the new solutions bifurcate from the Atkinson-Cabrera solutions at the velocity V_0 at which the latter become inadmissible. In Section 5 we describe the numerical procedure we use to obtain solutions in the case when z is not necessarily small. We use this procedure to generate new solutions in the low-velocity regime $0 < V < V_0$ and discuss their properties. We verify the numerical pro-

cedure by comparing it with the analytical method described in the Appendix and with the analytical results of Section 4. In Section 6 we investigate stability of the traveling wave solutions using numerical simulations of the discrete chain dynamics. The results suggest instability of the new solutions. Section 7 adds viscosity to the model. We find that this addition does not seem to stabilize slow new type traveling waves in general. The Appendix describes an analytical method for solving a version of the integral equation that arises here and in [15], with truncated kernel retaining a finite number of exponential terms, by converting it to a differential equation.

2 Atkinson-Cabrera traveling wave solutions

The dynamics of the driven Frenkel-Kontorova chain are described by the following equation, expressed in dimensionless quantities.

$$\ddot{u}_n = u_{n+1} - 2u_n + u_{n-1} + \mu(\sigma - \Phi'(u_n)). \tag{1}$$

Here $u_n(t)$ is the displacement of the nth mass at time t, μ is a ratio of stiffness of the nonlinear interaction with the substrate to nearest neighbor interactions and Φ is the multiple well substrate potential. To model a steadily moving dislocation, we seek solutions of (1) in the form of a traveling wave with (constant) velocity $V > 0$:

$$u_n = u(\xi), \quad \xi = n - Vt. \tag{2}$$

Substituting this ansatz in (1), we obtain the advance-delay differential equation

$$V^2 u'' = u(\xi + 1) - 2u(\xi) + u(\xi - 1) + \mu(\sigma - \Phi'(u(\xi))). \tag{3}$$

We are interested in solutions of (3) that are of *kink type*. These satisfy the following conditions at infinity:

$$\langle u(\xi) \rangle \to u_\pm \quad \text{as } \xi \to \pm\infty, \tag{4}$$

where $u_\pm$ are stable constant (uniform) equilibrium solutions of (3) located in two *different* wells:

$$\Phi'(u_\pm) = \sigma, \quad u_- > u_+, \quad \Phi''(u_\pm) > 0.$$

The angular brackets in (4) denote the average value of the displacement because we expect this Hamiltonian discrete system to develop oscillations. The average is taken over a sufficiently large interval.

Instead of the usual periodic potential, we choose a potential with only two wells; this is appropriate for describing *twinning dislocations*. As first shown in [1], an explicit

solution of (3), (4) can be obtained if one assumes that the substrate potential is piecewise quadratic:

$$\Phi(u) = \begin{cases} \frac{1}{2}(u+1)^2, & u \le 0 \\ \frac{1}{2}(u-1)^2, & u \ge 0. \end{cases} \tag{5}$$

Note that the derivative of this potential is discontinuous at $u = 0$:

$$\Phi'(u) = u - 2\theta(u) + 1, \tag{6}$$

where $\theta(u)$ is the unit step function: $\theta(u) = 1$ for $u > 0$, $\theta(u) = 0$ for $u < 0$. Observe also that in this case one has $u_\pm = \sigma \pm 1$ in (4).

Suppose that the displacement switches from the second to the first well at $\xi = 0$, so that

$$u(\xi) > 0 \quad \text{for } \xi < 0, \quad u(\xi) < 0 \quad \text{for } \xi > 0 \tag{7}$$

and

$$u(0) = 0. \tag{8}$$

Then one may replace $\theta(u(\xi))$ by $\theta(-\xi)$ in (6). Then (3) becomes a linear equation:

$$V^2 u'' = u(\xi+1) - (2+\mu)u(\xi) + u(\xi-1) + \mu(\sigma - 1 + 2\theta(-\xi)), \tag{9}$$

which can be solved using Fourier transforms.

It should be emphasized that solutions of (9) satisfy the original nonlinear equation (3) if and only if the *admissibility condition* (7) holds. Otherwise, if a solution of (9) violates (7) it will be labeled as *inadmissible*.

The solution of (9) constructed by Atkinson and Cabrera [1] (see also [3, 9] for more details) is as follows:

$$u = U(\xi) \equiv \begin{cases} \sigma - 1 - 2\mu \displaystyle\sum_{k \in M^+(V)} \frac{e^{ik\xi}}{kL_k(k,V)}, & \xi > 0 \\ \sigma + 1 + 2\mu \displaystyle\sum_{k \in M^-(V)} \frac{e^{ik\xi}}{kL_k(k,V)}, & \xi < 0. \end{cases} \tag{10}$$

Here

$$M^\pm(V) = \{k : L(k,V) = 0,\ \mathrm{Im}k \gtrless 0\} \cup N^\pm(V) \tag{11}$$

are the sets of roots of the dispersion relation $L(k,V) = 0$, where

$$L(k,V) = \mu + 4\sin^2\frac{k}{2} - V^2k^2, \tag{12}$$

with $L_k \equiv \partial L/\partial k$, while

$$N^\pm(V) = \{k : L(k,V) = 0,\ \mathrm{Im}(k) = 0,\ kL_k(k,V) \gtrless 0\} \tag{13}$$

denote the sets of real roots. The real roots correspond to lattice waves (phonons) emitted by the moving dislocation. The construction of $N^{\pm}(V)$ implies that corresponding modes propagate ahead or behind the dislocation in accordance with the radiation condition [1, 9]. This condition, also known as the causality principle [14], selects solutions such that in a frame moving with the dislocation, lattice waves can only be emitted by the moving front and must carry energy away from it (thus causing radiative damping). Thus phonon modes whose group velocity $V_g = V + L_k(k, V)/(2Vk)$ is less than the velocity V of the front must be placed behind it (the set $N^-(V)$ contributes to $\xi < 0$), while the modes with group velocity above V propagate ahead ($N^+(V)$).

The nonlinearity of the problem is contained in conditions (7) and (8). Applying (8), one obtains the *kinetic relation* between the applied stress and the dislocation velocity:

$$\sigma = \Sigma(V) \equiv 2\mu \sum_{k \in N(V)} \frac{1}{|kL_k(k, V)|}, \tag{14}$$

where the sum is over the set of all real roots, $N(V) = N^+(V) \cup N^-(V)$. Thus the applied stress is determined entirely by the real roots. As shown in [9], one can derive (14) by accounting for the energy fluxes carried by the phonon waves.

For a given $V > 0$ the solution is thus given by (10), (14), *provided* that the admissibility inequalities (7) are satisfied.

Computing the real roots of (12) for each $V > 0$, we formally obtain the kinetic relation (14), shown in Fig. 1a for the case of $\mu = 1$. The relation consists of disjoint segments separated by *resonance velocities*, i.e. values of V such that $L(k, V) = 0$ and $L_k(k, V) = 0$ for some real k (see Fig. 1b). A typical solution above the first resonance ($V = 0.5$) is shown in grey in Fig. 2a. One can see that a moving dislocation emits phonon oscillations behind it, with wave number equal to the single positive real root of (12). As velocity decreases below the first resonance (see the displacement profile at $V = 0.2$ in Fig. 2b), more oscillation modes appear, and $u(\xi)$ formally obtained from (10), (14) features phonon emission on both sides. However, closer inspection reveals that this solution of (9) is in fact *inadmissible* and should be removed because it violates the assumption that $u(\xi) < 0$ for $\xi > 0$ (one of the admissibility conditions (7)). In fact, numerical calculations of the solution U of (9) reveal that all segments of the kinetic relation below the first resonance contain only inadmissible traveling waves that change signs more than once, and thus need to be removed, while the remaining large-velocity segment contains admissible solutions above a certain threshold velocity [9]. In the case of $\mu = 1$, solutions of (9) are admissible for $V \geq V_0 \approx 0.357$. This implies non-existence of traveling wave solutions *under the assumptions* (7), (8) when the velocity is below the threshold value V_0. While this nonexistence issue was recognized by various authors [1, 5, 9, 3], it remains unclear whether there exist any moving kink type solutions below the threshold velocity. This paper addresses this question.

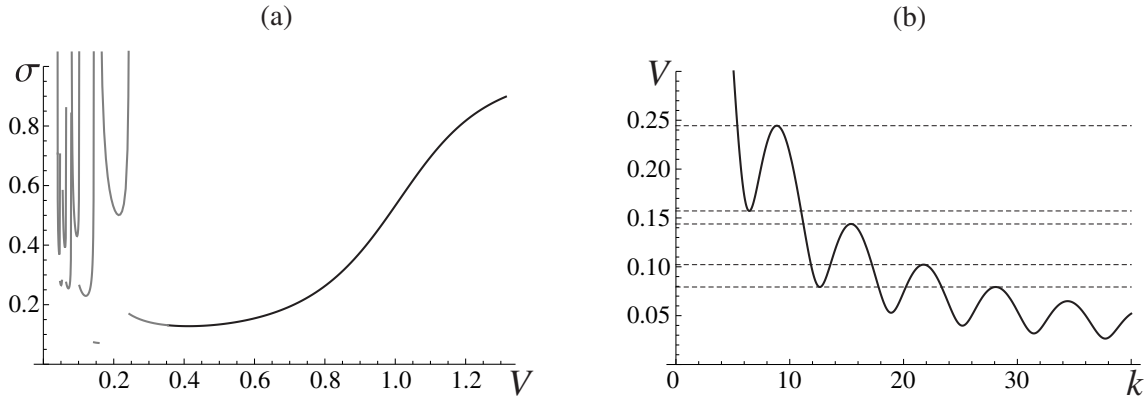

Figure 1: (a) Kinetic relation resulting from the formally obtained Atkinson-Cabrera solution. Only the first twelve segments are shown. The grey curves correspond to inadmissible traveling waves. (b) Solutions of $L(k, V) = 0$ for positive real k. The dashed lines indicate the first five resonance velocities at which $L_k(k, V) = 0$. Here $\mu = 1$.

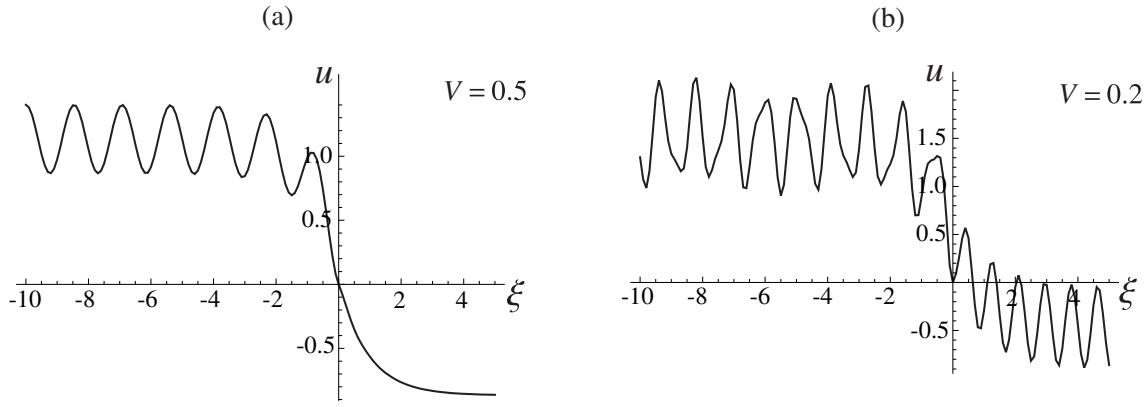

Figure 2: Displacement profiles formally computed from (10), (14) at (a) $V = 0.5$ and (b) $V = 0.2$. Solution in (a) satisfies the constraints (7) but the one in (b) does not. Here $\mu = 1$.

3 New traveling wave solutions

To obtain valid traveling wave solutions of (3) in the low-velocity regime, we now replace the admissibility conditions (7), (8) by a more general assumption

$$\begin{aligned} u(\xi) &> 0, \quad \xi < -z \\ u(\xi) &= 0, \quad |\xi| \leq z \\ u(\xi) &< 0, \quad \xi > z, \end{aligned} \tag{15}$$

where $z > 0$ is to be determined. In other words, we assume that instead of switching wells instanteneously at $t = n/V$ ($\xi = 0$), the nth particle may stay at the spinodal value $u = 0$ between the wells over the time period $[(n - z)/V, (n + z)/V]$ ($|\xi| \leq z$). For $z = 0$ we recover Atkinson-Cabrera solutions.

Adopting a method used in [7, 15], we observe that $\Phi'(u(\xi))$ can now be written as

$$\Phi'(u(\xi)) = u(\xi) + 1 - 2\int_{-z}^{z} h(s)\theta(s - \xi)ds, \tag{16}$$

where we have introduced an unknown shape function $h(s)$, which vanishes outside the interval $[-z, z]$ and is normalized so that

$$\int_{-z}^{z} h(s)ds = 1. \tag{17}$$

Thus we obtain

$$V^2u'' + (\mu + 2)u(\xi) - u(\xi + 1) - u(\xi - 1) = \mu\left[\sigma - 1 + 2\int_{-z}^{z} h(s)\theta(s - \xi)ds\right]. \tag{18}$$

For consistency, we must require that in addition to (18) and (4), the solution satisfies the *generalized admissibility conditions* (15).

Taking the Fourier transform of (18) and using the convolution theorem, one can show (see [7, 16] for details) that

$$u'(\xi) = -\int_{-z}^{z} h(s)q(\xi - s)ds, \tag{19}$$

where the kernel is the negative derivative of the solution (10) of (9) with $z = 0$:

$$q(\xi) = -\frac{dU}{d\xi} = \begin{cases} 2\mu i \sum\limits_{k \in M^+(V)} \dfrac{e^{ik\xi}}{L_k(k, V)}, & \xi > 0 \\ -2\mu i \sum\limits_{k \in M^-(V)} \dfrac{e^{ik\xi}}{L_k(k, V)}, & \xi < 0. \end{cases} \tag{20}$$

At the same time, our assumption that $u(\xi) \equiv 0$ at $|\xi| \leq z$ implies that $u'(\xi) \equiv 0$ in the interval $(-z, z)$. Together with (19), this yields the integral equation

$$\int_{-z}^{z} h(s)q(\xi - s)ds = 0, \quad |\xi| < z. \tag{21}$$

Thus the shape function $h(\xi)$ is an eigenfunction of the integral operator in the left hand side of (21) (with kernel given by (20)) associated with the zero eigenvalue. As described in more detail in Section 4, the integral operator has a zero eigenvalue provided that z takes on special values. Note that (21) is a Fredholm integral equation of the first kind. We remark that if instead of (6) one considers a trilinear (continuous) $\Phi'(u)$,

$$\Phi'(u) = \begin{cases} u + 1, & u < -\gamma/2 \\ (1 - 2/\gamma)u, & |u| \leq \gamma/2 \\ u - 1, & u > \gamma/2, \end{cases}$$

the same procedure yields a Fredholm integral equation of the second kind, with the right hand side of (21) replaced by $\gamma h(\xi)$, where γ is the width of the spinodal region connecting the two wells [15] (see also related problems with different kernels in [7, 16]). In the limit $\gamma \to 0$ one recovers (21).

The problem thus reduces to solving the integral equation (21) for z and $h(\xi)$. Once $h(\xi)$ and z are known, the convolution theorem yields the traveling wave solution:

$$u(\xi) = \sigma - \Sigma(V) + \int_{-z}^{z} h(s)U(\xi - s)ds, \tag{22}$$

where the applied stress

$$\sigma = \Sigma(V) - \frac{1}{2}\int_{-z}^{z} h(s)(U(z - s) + U(-z - s))ds \tag{23}$$

is found by applying $u(z) = u(-z) = 0$. If $z = 0$, the shape function reduces to the Dirac delta function $h(s) = \delta(s)$, and (22), (23) reduce to (10), (14), respectively.

We will present numerical evidence that this procedure yields valid traveling waves (solutions of (3)) for values of V where the Atkinson-Cabrera solution U of (9) is inadmissible. This is due to the fact that for such values of V, $u(\xi)$ given by (22) conforms to the generalized admissibility conditions (15).

4 Kernel approximations for small z and bifurcation

Using an approximation of the integral operator in (21), we show that the new type of traveling waves with $z > 0$ bifurcate from the Atkinson-Cabrera solutions precisely at

the threshold velocity V_0, below which the latter become inadmissible. The conditions near bifurcation thus involve values of z near 0. This suggests that in order to study the problem analytically, we may replace the kernel q in (21) on $[-z, z]$ by its piecewise linear approximation near zero, as in [7]. We note that $q(\xi)$ is continuous, while $q'(\xi)$ has a jump discontinuity at $\xi = 0$, as can be shown from (9), since $q(\xi) = -U'(\xi)$. Let

$$\hat{q}(\xi) = \begin{cases} q_0 + q_+\xi, & \xi > 0 \\ q_0 + q_-\xi, & \xi < 0, \end{cases} \tag{24}$$

where

$$q_0 = q(0), \quad q_\pm = q'(0\pm), \quad q_+ - q_- = 2\mu/V^2; \tag{25}$$

the last relation is implied by (9). Here $\hat{q}$ is a piecewise linear approximation of q near zero. Consider the approximate version of (21) given by $\int_{-z}^{z} h(s)\hat{q}(\xi - s)ds = 0$, $|\xi| < z$. It turns out that the only L^1 solution of this is the trivial one. To see this, note that $\int_{-z}^{z} h(s)\hat{q}(\xi - s)ds$ can be differentiated twice with respect to ξ, with second derivative equal to $(q_+ - q_-)h(\xi)$ ($|\xi| < z$), which therefore has to vanish. In contrast with [15], we are led to seek generalized solutions involving delta functions [13]. One way to approach this is to study solutions of the corresponding equation of the second kind, which actually arises in [15],

$$\int_{-z}^{z} h(s)\hat{q}(\xi - s)ds - \gamma h(\xi) = 0, \quad |\xi| < z, \tag{26}$$

with γ a positive constant, and then take the limit as $\gamma \to 0+$. Assuming h is smooth enough, differentiate (26) twice to find that h must satisfy the ODE

$$\gamma h''(\xi) - (q_+ - q_-)h(\xi) = 0, \quad |\xi| < z.$$

Inserting the general solution of this,

$$h(\xi) = c_1 e^{\xi/a} + c_2 e^{-\xi/a}, \quad a = \sqrt{\gamma/(q_+ - q_-)}, \tag{27}$$

into (26) and evaluating the integral, we obtain an expression linear in ξ, which must vanish for $|\xi| < z$. This yields a homogeneous linear system for the constants c_1 and c_2, which has nontrivial solutions, provided that the corresponding determinant vanishes. This can be put into the form of a quadratic equation in the quantity $e^{2z/a}$, whose coefficients depend on z and γ. Solving this quadratic gives the following equations:

$$e^{2z\sqrt{(q_+ - q_-)/\gamma}} = \frac{B_\pm(z, \gamma)}{A(z, \gamma)}, \tag{28}$$

where

$$B_\pm(z, \gamma) = -a\left({q_-}^2 + {q_+}^2\right) \\ \pm \sqrt{(q_- - q_+)^2\left({q_0}^2 + a^2(q_- + q_+)^2\right) + 4q_0 q_-(q_- - q_+)q_+ z + 4{q_-}^2{q_+}^2 z^2}$$

and

$$A(z,\gamma) = q_0(q_- - q_+) + 2q_-q_+(z-a),$$

with a as in (27). Note that A, $B_\pm$ are continuous algebraic functions, which thus remain bounded for finite values of their arguments. This provides a relation between z and γ. Suppose that z tends to a positive value as $\gamma \to 0+$. Then the left hand side of (28), hence also the right hand side, grows unbounded. This necessitates that the denominator $A \to 0$, or passing to the limit, $A(z,0) = 0$, which reduces to

$$z = \frac{q_0(q_+ - q_-)}{2q_+q_-}. \tag{29}$$

From (20) and the last of (25) one shows that $(q_+ - q_-)/(2q_+q_-) < 0$. Positive solutions z of (29) exist provided $-q_0 = U'(0) > 0$. On the other hand, the admissibility conditions (7) for U imply that $U'(0) \le 0$. This provides strong analytical evidence that bifurcation to the new type of traveling wave with $z > 0$ occurs precisely at the threshold velocity V_0, at which the Atkinson-Cabrera solution becomes inadmissible. In the next section we show this numerically as well using the full kernel.

For small $\gamma > 0$ one can fully determine the constants c_1, c_2 and z in terms of γ by enforcing the normalization condition (17). The result can be put into the form

$$h(\xi) = \frac{q_- \cosh\left(\frac{\xi - z}{a}\right) - q_+ \cosh\left(\frac{\xi + z}{a}\right)}{a(q_- - q_+)\sinh\left(\frac{2z}{a}\right)}.$$

It is straightforward to show that the limit as $\gamma \to 0+$ is

$$h(\xi) = \frac{q_-}{(q_- - q_+)}\delta(\xi + z) - \frac{q_+}{(q_- - q_+)}\delta(\xi - z), \tag{30}$$

in the sense of distributions (with delta functions at $\pm z$). One can show this directly by substituting the ansatz $h(\xi) = \alpha_+\delta(\xi+z) + \alpha_-\delta(\xi - z)$ (with $\alpha_\pm$ unknown constants) into the first-kind approximate equation $\int_{-z}^{z} h(s)\hat{q}(\xi - s)ds = 0$, $|\xi| < z$. This determines $\alpha_\pm$ and yields (29) and (30).

One shows that even derivatives of q are continuous at 0. If we add a quadratic term $q_2\xi^2$ to the piecewise linear kernel approximation (24), the above procedure can be repeated with similar results. The analogue of (30) now takes the form

$$h(\xi) = \alpha_+\delta(\xi+z) + \alpha_-\delta(\xi - z) + \zeta, \quad \zeta = \frac{2q_2}{q_+ - q_-}, \quad \alpha_\pm = \frac{q_+ - q_- - 4q_2z}{2(q_+ - q_-)} \mp \frac{q_+ + q_-}{2(q_+ - q_- + 4q_2z)}$$

and z is a root of the quartic equation

$$(q_+ - q_-)q_0 + (4q_2q_0 - 2q_+q_-)z - \frac{32q_2^2}{3}z^3 - \frac{32q_2^3}{3(q_+ - q_-)}z^4 = 0.$$

Note that for $q_2 = 0$ the last two equations reduces to (30) and (29). It turns out that only the smallest positive root z of this quartic equation gives rise to traveling waves satisfying the generalized admissibility conditions (15); this root is well approximated by that of (29).

Another possibility is to consider a kernel in the form of a sum of exponentials, but containing only a finite number N of terms from (20). In that case, (21) can be solved analytically. The procedure is described in detail in the Appendix and is not confined to the case of small z. Unfortunately, this approach involves matrix computations that become progressively more difficult computationally as N is increased. Instead, in the following section we solve (21) numerically, using the analytical method of the Appendix to validate our numerical computations.

5 Numerical results

We now consider the general case where z is not necessarily small.

For given $V > 0$, the solution $h(\xi)$ and z of (21) was found numerically as follows. Since there are infinitely many roots of (12), it was necessary to approximate the kernel (20) by retaining the first N roots of (12) nearest the origin. To get an accurate approximation of the kernel $q(\xi)$ near $\xi = 0$, it was necessary to include a large number of roots ($N = 400$ was typically used). The trapezoidal approximation of the integral equation for a finite z (with 400 uniformly distributed mesh points) then yielded a homogeneous linear system $\mathbf{Q}(z)\mathbf{h} = \mathbf{0}$. Here $\mathbf{h}$ is the vector of values of $h(s)$ at the mesh points. Solving $\det\mathbf{Q}(z) = 0$ for z, we obtained the corresponding $\mathbf{h}$ normalized to satisfy (17) in the sense of the trapezoidal approximation. In general, there were more than one root of $\det\mathbf{Q}(z) = 0$, but at most one of these yielded admissible solutions that satisfied the generalized admissibility conditions (15) within numerical error. Once the admissible z and $\mathbf{h}$ were found, the trapezoidal approximation of the integrals in (22) and (23) was used to compute the solution $u(\xi)$ and the applied stress σ. Fig. 3 shows the solution $u(\xi)$ obtained at $V = 0.2$ and $\mu = 1$ (black curve) along with the inadmissible Atkinson-Cabrera solution $U(\xi)$ ($z = 0$, grey curve). In this case $z = 0.21$. One can see that the obtained solution satisfies the constraints (15) within numerical error (which is of the order of 10^{-7} in this case).

Repeating this procedure for a range of velocities, we obtain the kinetic relation $\sigma(V)$ and the corresponding relation $z(V)$ between z and V shown in Fig. 4. Note that $z(V)$ decreases as V grows and becomes zero at $V = V_0 \approx 0.357$. This is the threshold velocity such that $q(0) = 0$, which equals the bifurcation velocity as predicted in Sec. 4. At $V \geq V_0$, the Atkinson-Cabrera solutions are admissible, and we have $z = 0$ and $\sigma = \Sigma(V)$ (thick segments in Fig. 4). Interestingly, for V below V_0 we obtained admissible solutions with $z > 0$ even in the immediate vicinity of the *resonance velocities*. At these velocities,

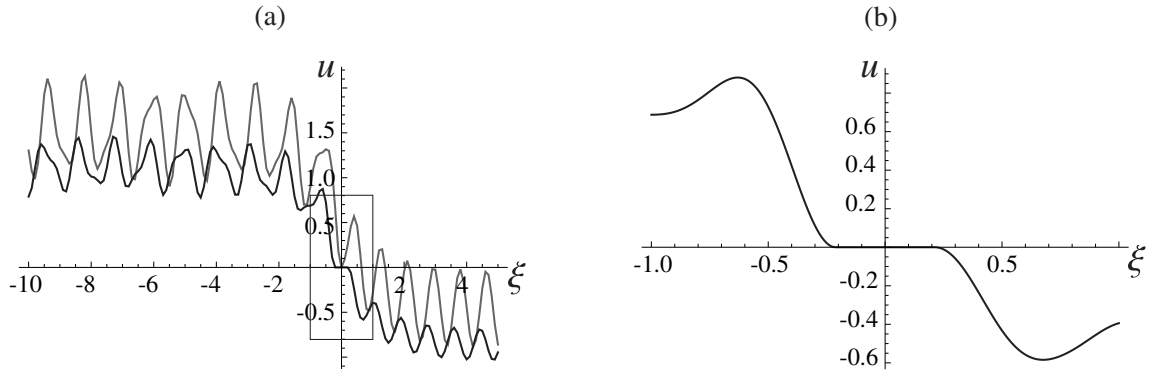

Figure 3: (a) Traveling wave solution $u(\xi)$ at $V = 0.2$, $\mu = 1$ with $z = 0.21$ (black curve), shown together with inadmissible $z = 0$ solution U (grey curve). (b) Zoom-in of the $z = 0.21$ solution inside the rectangle in (a).

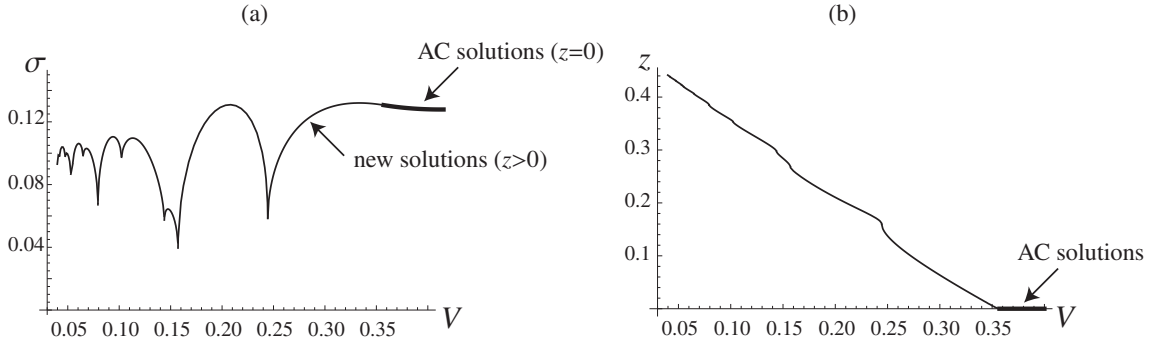

Figure 4: (a) Kinetics relation $\sigma(V)$ and (b) the corresponding $z(V)$ at $\mu = 1$. The thicker segments above the threshold velocity $V_0 \approx 0.357$ indicate the parts of the curves that correspond to Atkinson-Cabrera solutions ($z = 0$).

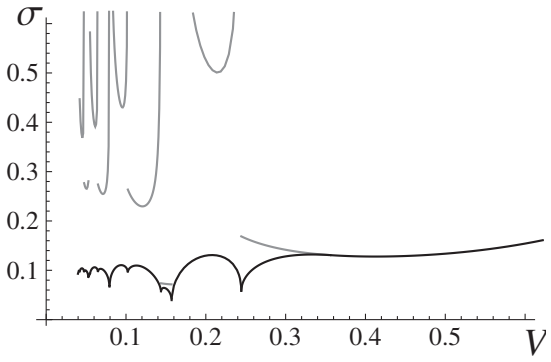

Figure 5: Comparison of the kinetic relation $\sigma(V)$ (black curve) generated by the new solutions to the relation $\Sigma(V)$ (grey lines) obtained from Atkinson-Cabrera solutions. The two curves coincide above the threshold velocity $V_0 \approx 0.357$. The grey curve corresponds to *inadmissible* Atkinson-Cabrera solutions below V_0. Here $\mu = 1$.

the Atkinson-Cabrera kinetic relation $\Sigma(V)$ is inadmissible and has singularities, while the kinetic relation $\sigma(V)$ based on the present admissible solutions has cusps; see Fig. 5.

The computed shape function $h(s)$ corresponding to velocity $V = 0.353$ ($z = 0.0026$) is shown in Fig. 6a. Note that it approximates the delta-function behavior at $s = \pm z$ that was predicted in Sec. 4. As V decreases, the shape functions develop oscillations due to the increasingly oscillatory behavior of $q(\xi)$ at smaller V; see, for example, Fig. 6b for $h(s)$ at $V = 0.2$, which corresponds to the solution shown in Fig. 3.

To see the effect of the number of roots included in the truncated kernel, we repeated the simulation with $N = 40$ roots. The resulting kinetic relations are compared in Fig. 7a,b. One can see that the two relations are very close everywhere except at quite small velocities $V < 0.05$, where inclusion of only 40 roots does not approximate the Atkinson-Cabrera solution well enough. In contrast, there is a noticeable difference between the corresponding $z(V)$ curves (see Fig. 7c). The lower values of z when fewer roots are included are due to the slow convergence of the kernel $q(\xi)$ in (20) near $\xi = 0$. In particular, one obtains a lower threshold value V_0, where z becomes zero, as the number of roots in the truncated kernel is decreased.

Nevertheless, we can use computations with a small number of roots to verify our numerical procedure by comparing shape functions computed numerically with the ones obtained using the semi-analytical method described in the Appendix. The results for $N = 8$ and $N = 44$ roots are shown in Fig. 8, where the numerical results (thin curves) are compared to the regular part $h_0(x)$ of the semi-analytical shape function $h(x) = \alpha_+\delta(x + z) + \alpha_-\delta(x - z) + h_0(x)$, shown by the thick curve, at $V = 0.245$. One can see

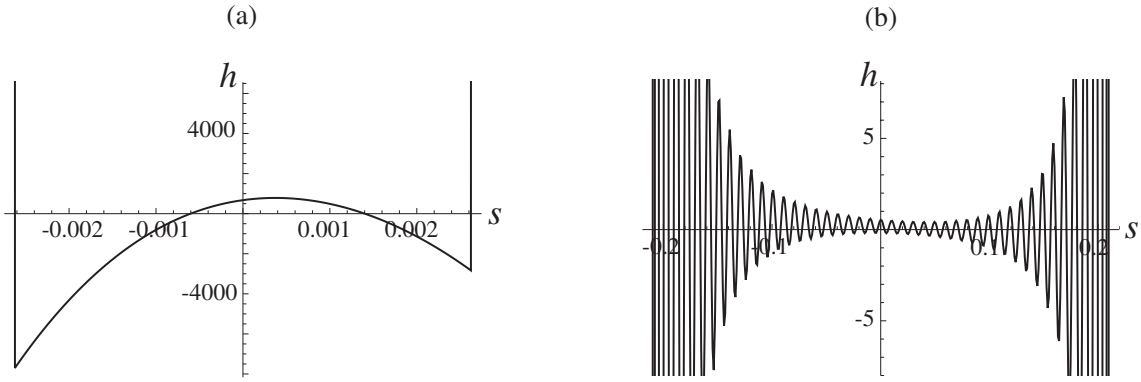

Figure 6: Shape functions $h(s)$ in the interval $[-z, z]$ at (a) $V = 0.353$, $z = 0.0026$ and (b) $V = 0.2$, $z = 0.21$. Here $\mu = 1$.

that the shape functions obtained using the two methods agree very well (the difference is below 0.0004% in (a) and 0.007% in (b)). Observe, however, that including more roots resulted in a more oscillatory function and, as remarked above, higher value of z.

Finally, we consider the bifurcation diagram for $z(V)$ near the threshold velocity V_0. To obtain accurate results near this threshold, one needs to include an even larger number of roots in the truncated kernel that approximates (20). Instead, we compute $q(\xi)$ using numerical evaluation of the integral representation of the kernel without truncating roots, and compare the resulting $z_N(V)$ obtained using the trapezoidal rule (solid curve) to the curve $z_L(V)$ obtained from (25) using the linear approximation of the kernel (dashed line) in Fig. 9. As one can see, the two curves become closer as we approach the threshold velocity from below.

6 Stability of traveling wave solutions

To investigate the stability of the new type of traveling waves, we conducted a series of numerical simulations, since in general it is quite difficult to check stability of traveling waves analytically [2]. For a given applied stress σ, we used the Verlet algorithm (a symplectic scheme) to solve the system (1) of ordinary differential equation for a truncated lattice with N masses, ranging from $N = 600$ to 2000, depending on the time of the simulation. A longer chain was used if the simulation ran for a long time, in order to avoid reflection of elastic waves from the domain boundaries. The boundary conditions were $u_0 = \sigma + 1$ and $u_N = \sigma - 1$. Two types of initial conditions were used. The first one

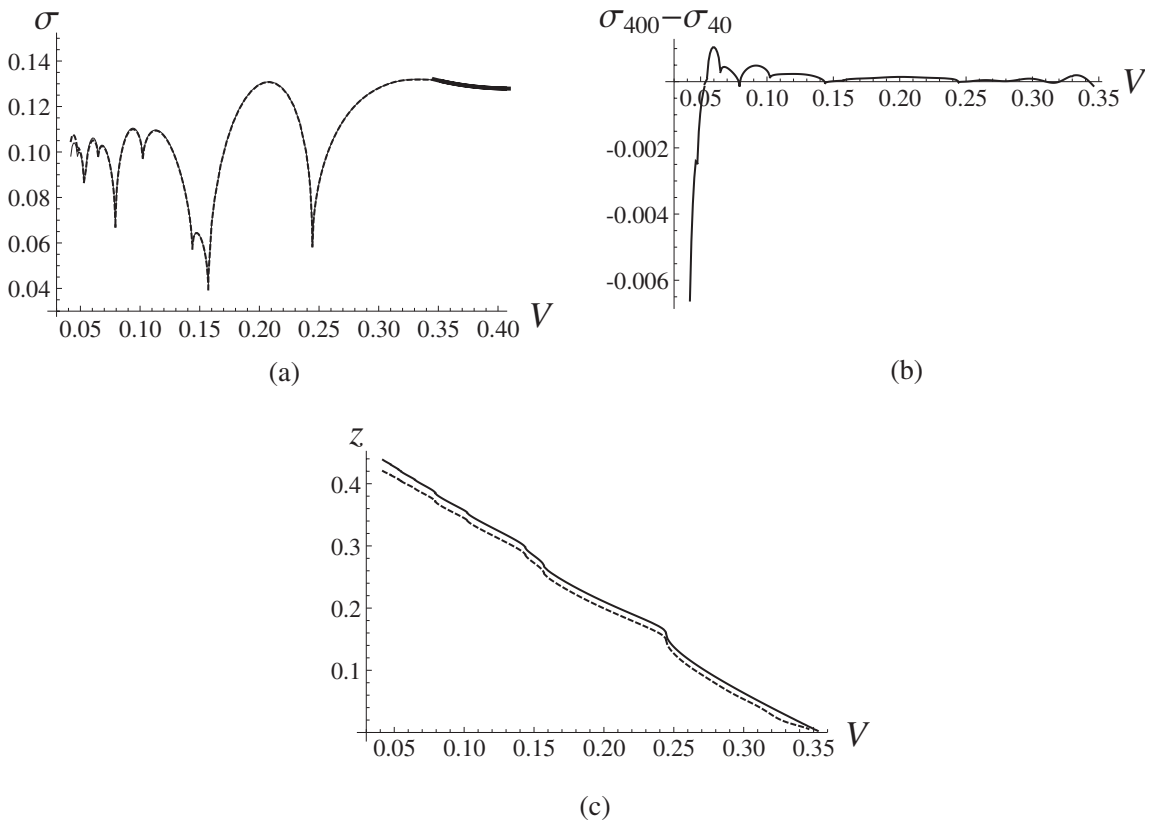

Figure 7: (a) Comparison of the numerical results at $\mu = 1$ obtained using the truncated kernel with $N = 400$ (solid curves) and $N = 40$ roots (dashed curves): (a) kinetic relations $\sigma(V)$; (b) the difference between the two relations; (c) the corresponding $z(V)$ curves.

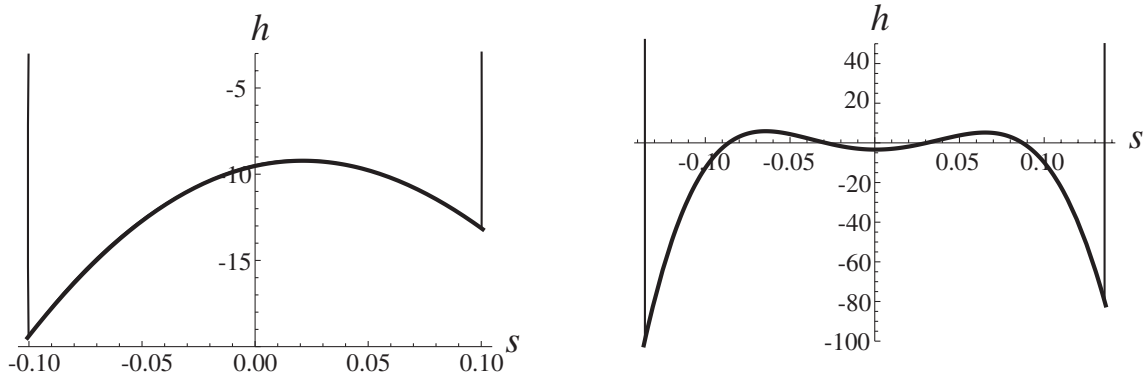

Figure 8: Comparison of the numerically computed shape functions $h(s)$ in the interval $[-z, z]$ at $V = 0.245$ (thin curves) and the regular part of the shape functions obtained using the semi-analytical method described in the Appendix (thick curves) including (a) 8 roots ($z = 0.1006$) and (b) 44 roots ($z = 0.1363$). Here $\mu = 1$.

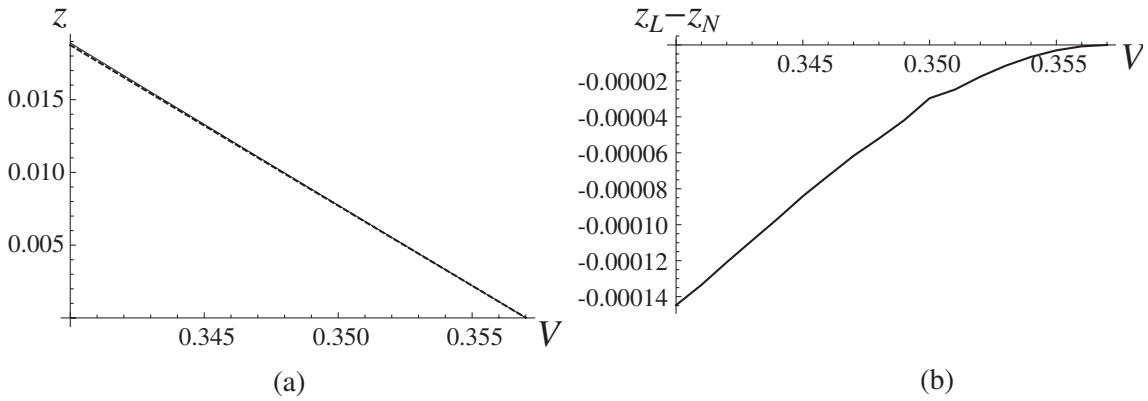

Figure 9: Comparison of the function $z_N(V)$ computed numerically using the full kernel (solid line) and $z_L(V)$ obtained from (25) using the linear approximation of the kernel (dashed line) near the bifurcation point $V_0 \approx 0.357$. Here $\mu = 1$.

was Riemann-type piecewise constant initial displacement and zero initial velocity:

$$(u_n(0), \dot{u}_n(0)) = \begin{cases} (\sigma + 1, 0) & 0 \le n < n_0 \\ (0, 0), & n = n_0, \\ (\sigma - 1, 0), & n_0 < n \le N \end{cases} \tag{31}$$

where $n_0 = N/2$ for even N. Numerical simulations with these initial data sought to identify stable states at a given loading that have a relatively wide basin of attraction. To capture other possibly stable states that coexist with solutions found using (31) but have a more narrow basin of attraction, and to identify solutions that are likely to be unstable, we used a second type of initial conditions, that were built from the obtained traveling wave profiles $u_n(t) = u(n - Vt)$:

$$(u_n(0), \dot{u}_n(0)) = \begin{cases} (\sigma + 1, 0) & 0 \le n < p \\ (u(n - n_0), -Vu'(n - n_0)) & p \le n \le N - p. \\ (\sigma - 1, 0) & N - p < n \le N \end{cases} \tag{32}$$

The truncated traveling wave solutions were surrounded by intervals of constant displacement of appropriately chosen size $p < n_0$ in order to ensure compatibility with the boundary conditions and avoid wave reflection from the boundaries. In both types of simulations, after a sufficiently long time, the solution approached an attractor corresponding to either a stationary dislocation (zero velocity) or a steadily moving front.

The results are shown in Fig. 10. One can see that when the applied stress is below a certain threshold $\sigma_{\rm D}$ (here $\sigma_{\rm D} = 0.128$), the long-time solution features a stationary front. For example, in the simulations with piecewise-constant initial conditions (31) the front propagates for some time (which increases as we approach the σ_D from below) and then becomes stationary. This is ullustrated in Fig. 11, which shows the position $\nu(t)$ of the front (defined as the value of n such that $u_n(t) > 0$ and $u_{n+1}(t) < 0$) at $\sigma = 0.125$ and $\sigma = 0.1275$. In general, stable stationary solutions exist when σ is inside the trapping region $|\sigma| \le \sigma_{\rm P}$, where $\sigma_{\rm P} = \sqrt{\mu/(4 + \mu)}$ (≈ 0.447 for $\mu = 1$) is the Peierls stress [17]. The fact that $\sigma_D < \sigma_P$ has been observed in earlier works, e.g. [5, 3]. The trapping region is marked by a thick segment along $V = 0$ in Fig. 10.

When stress is above the threshold value ($\sigma \ge \sigma_{\rm D}$), the solution approaches a steady dislocation motion after some time. For example, at $\sigma = 0.14$, the long-time solution features the dislocation moving steadily with velocity $V = 0.54$; see Fig. 12. Comparison of the numerical solution zoomed in around the front (circles) and the corresponding traveling wave solution (solid curve) in Fig. 12b shows excellent agreement, indicating stability of the traveling wave. In general, our simulations indicate that at stresses above $\sigma_{\rm D}$ all traveling waves are stable. Note that the threshold value $\sigma_{\rm D}$ (the dynamic Peirels

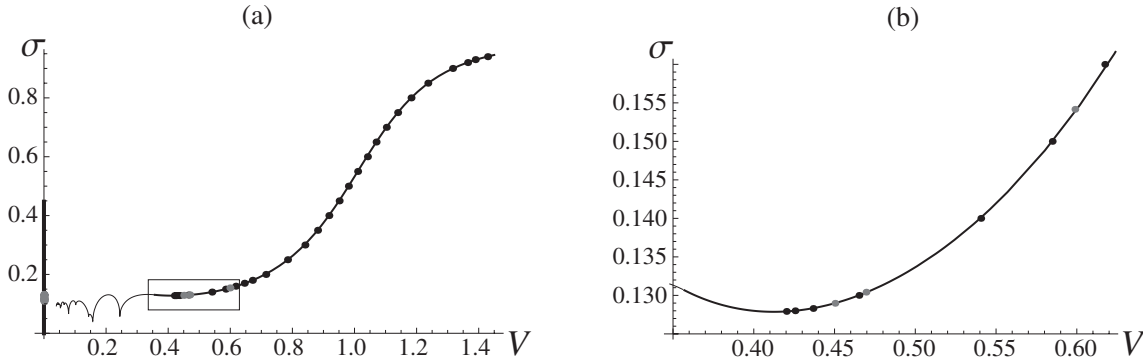

Figure 10: (a) Results of the numerical simulations at $\mu = 1$ with initial data (31) (black circles) and (32) (grey circles), shown together with the kinetic curve. (b) Zoom-in inside the rectangle in part (a). Thick black segment along $V = 0$ axis indicates the trapping region. Thinner portion of the kinetic curve corresponds to the solutions with $z > 0$.

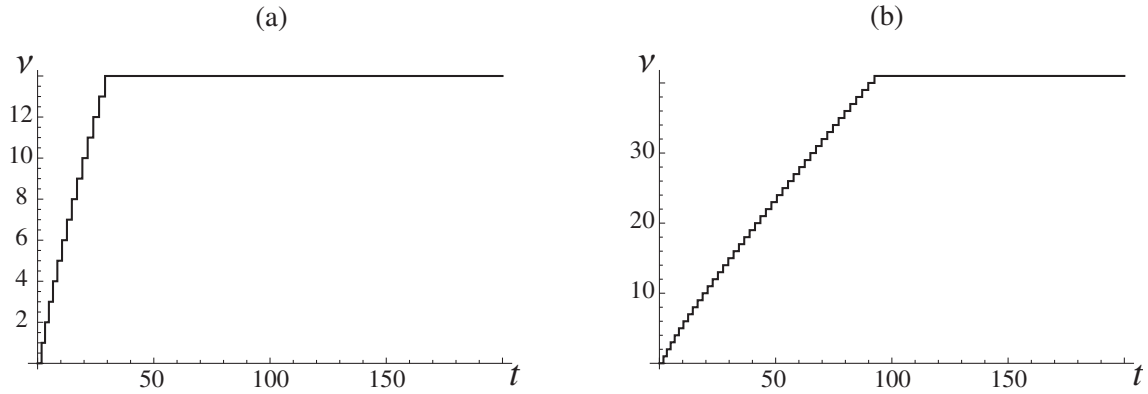

Figure 11: Position $\nu(t)$ of the dislocation at (a) $\sigma = 0.125$ and (b) $\sigma = 0.1275$ in the numerical simulations. Here $\mu = 1$.

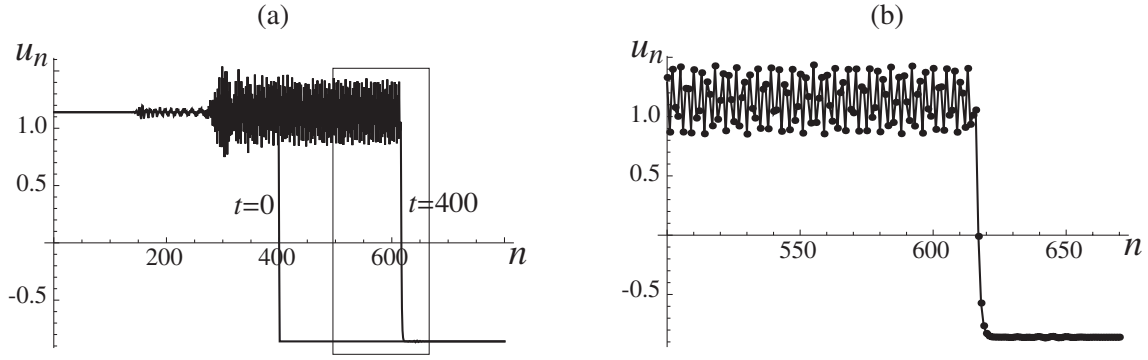

Figure 12: (a) Displacement profiles (solid lines) at $t = 0$ and $t = 400$ for the numerical simulation at $\mu = 1$ and $\sigma = 0.14$. (b) The numerical solution (circles) at $t = 600$ zoomed in around the dislocation front and compared to the traveling wave solution (solid curve) with the same velocity, $V = 0.54$.

stress) corresponds to a local minimum of the kinetic curve, as hypothesized in [1], and is *below* the Peierls stress $\sigma_{\rm P}$, implying that stable stationary states and stable steady motion coexist at stresses between the two values. Similar stability results were reported in [3] for simulations that include a viscosity term. A proof of stability of traveling waves with sufficiently high velocities, which for technical reasons does not extend to the whole $\sigma \geq \sigma_{\rm D}$ region, can be found in [2].

Note that inside the stability interval $\sigma \geq \sigma_{\rm D}$ suggested by the numerical simulations, all traveling waves have $z = 0$. Under initial data (32) based on the new-type traveling wave solutions with $z > 0$, numerical simulations always converged to attractors with stationary fronts. Our results thus suggest that such solutions are likely to be unstable. We remark, however, that some low-velocity solutions apparently become stable when a sufficiently wide spinodal region is included [11, 15].

7 Effect of viscosity

We now consider the effect of adding viscosity to the model on kink solutions and their stability. The rescaled governing equations become

$$\ddot{u}_n + \alpha\dot{u}_n = u_{n+1} - 2u_n + u_{n-1} + \mu(\sigma - \Phi'(u_n)), \tag{33}$$

where $\alpha > 0$ is the dimensionless viscosity coefficient. Traveling wave solutions are given by (10), (14) for $z = 0$ and by (22), (23) for $z > 0$, with (12) replaced by

$$L(k, V) = \mu + 4\sin^2\frac{k}{2} - V^2k^2 - ik\alpha V. \tag{34}$$

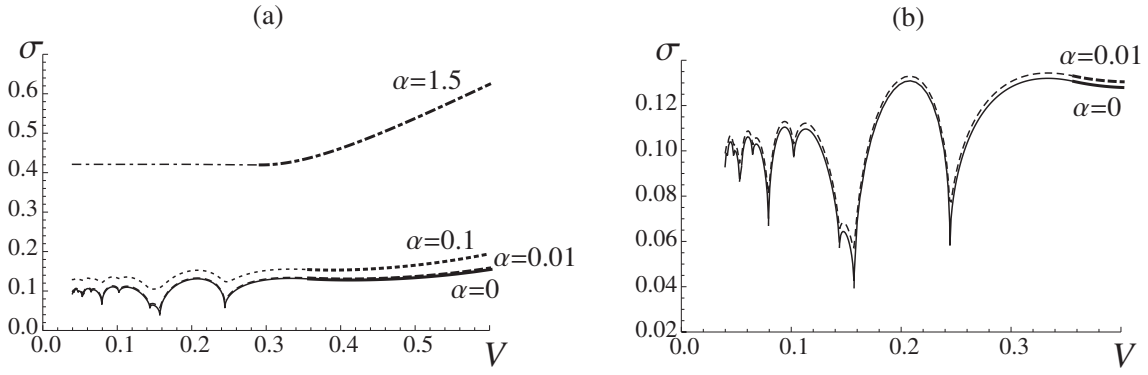

Figure 13: (a) Kinetic relation $\sigma(V)$ at $\mu = 1$ and different values of the viscosity coefficient α. (b) Zoom-in on the curves with $\alpha = 0$ and $\alpha = 0.01$. Thicker portions of the kinetic curves correspond to solutions with $z = 0$.

In this case there are no real roots; at small α the roots shift away from the real axis into upper and lower halves of the complex plane according to the radiation condition [9].

The effect of viscosity on the kinetic relation is shown in Fig. 13. As expected, viscosity smoothens the cusps at the resonance velocities. The amplitude of oscillations that are very pronounced in the kinetic curves at small α decreases as α increases; the velocity V_0 at which $z = 0$ solutions become admissible decreases as well. See also the corresponding $z(V)$ graph in Fig. 14a. At sufficiently large α we have $V_0 = 0$, so that all $z = 0$ solutions become admissible.

The value of V_0 also becomes smaller as we decrease μ, as shown in Fig. 14b. Another effect of the parameter μ is the different values of the resonance velocities.

The stability picture is not significantly affected by α and μ. See, for example, Fig. 15, where $\mu = 0.5$ and $\alpha = 0.1$. As before, only sufficiently fast $z = 0$ solutions, above the last local minimum of the kinetic curve, appear to be stable.

Acknowledgements

This research was partially supported by the European Union's Seventh Framework Programme (FP7-REGPOT-2009-1) under grant no. 245749 through the Archimedes Center for Modeling, Analysis and Computation (ACMAC) of the Department of Applied Mathematics at the University of Crete. The work of A.V. was supported by the U.S. National Science Foundation through grant DMS-1007908. A.V. thanks ACMAC and the Department of Applied Mathematics at the University of Crete for hospitality.

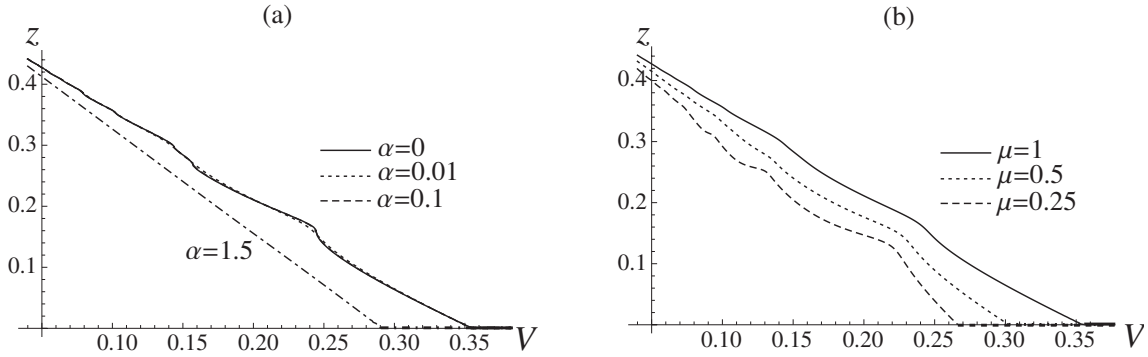

Figure 14: (a) $z(V)$ at $\mu = 1$ and different values of the viscosity coefficient α corresponding to the kinetic curves in Fig. 13. (b) $z(V)$ at $\alpha = 0.1$ and different values of μ.

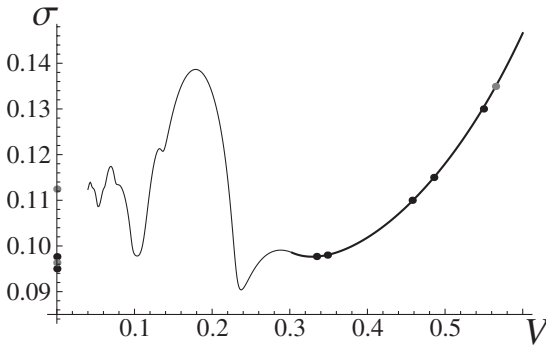

Figure 15: Results of the numerical simulations at $\mu = 0.5$ and $\alpha = 0.1$ with initial data (31) (black circles) and (32) (grey circles), shown together with the kinetic curve. Thinner portion of the kinetic curve corresponds to the solutions with $z > 0$.

A Appendix: Exact solution of the integral equation with truncated exponential kernel

Suppose that in (11) we truncate the roots so that we keep an equal number of complex roots in $M^+(V)$ and $M^-(V)$. Due to the presence of real roots, $M^+(V)$ and $M^-(V)$ will contain a different number of roots of $L(\kappa, V) = 0$. Suppose that after truncation we keep a total number N of roots κ_n, M of which are in $M^+(V)$ and $N - M$ are in $M^-(V)$, i.e.,

$$\kappa_n \in \begin{cases} M^+(V) & \text{for } n = 1, \dots, M, \\ M^-(V) & \text{for } n = M+1, \dots, N \end{cases} \tag{A.1}$$

Let

$$k_n = i\kappa_n, \quad A_n = 2\mu i / L_\kappa(\kappa_n, V) \tag{A.2}$$

and define, in view of (20),

$$q(\xi) = \begin{cases} q_+(\xi) = \sum\limits_{n=1}^{M} A_n e^{k_n \xi}, & \xi > 0, \\ q_-(\xi) = \sum\limits_{n=M+1}^{N} (-A_n) e^{k_n \xi}, & \xi < 0. \end{cases} \tag{A.3}$$

Because $q(\xi)$ is not smooth at 0, we observe that

$$\int_{-z}^{z} q(\xi - s) h(s) ds = \int_{-z}^{\xi} q_+(\xi - s) h(s) ds + \int_{\xi}^{z} q_-(\xi - s) h(s) ds,$$

and each of the last two integrals has a C^∞ kernel and can be differentiated. The same is true for the integrals

$$\begin{aligned} I_n(\xi) &= \int_{-z}^{\xi} A_n e^{k_n(\xi - s)} h(s) ds, \quad n = 1, \dots, M, \\ I_n(\xi) &= \int_{\xi}^{z} (-A_n) e^{k_n(\xi - s)} h(s) ds, \quad n = M+1, \dots, N. \end{aligned} \tag{A.4}$$

In view of them and (A.2), (A.3), the integral equation $\int_{-z}^{z} q(\xi - s) h(s) ds = f(\xi)$ becomes

$$\sum_{n=1}^{N} I_n(\xi) = f(\xi), \quad |\xi| < z, \tag{A.5}$$

where f is either identically zero or a given function or γh for the problem considered in [15] and here in Section 4. Differentiate (A.4) with respect to ξ using the Leibnitz Rule to find

$$I_n'(\xi) = A_n h(\xi) + k_n I_n(\xi). \tag{A.6}$$

Then differentiate the integral equation (A.5) and use (A.6) to eliminate I_n'. Repeat $N-1$ times so that together with (A.5) we have N equations where we have used (A.6) to eliminate I_n' after each differentiation [12]. Letting

$$f^{(m)}(\xi) = d^m f(\xi)/d\xi^m$$

for $m = 0, 1, \ldots$, the resulting system of N equations for I_n is

$$\sum_{n=1}^{N} k_n^{m-1} I_n(\xi) = f^{(m-1)}(\xi) - \sum_{p=1}^{m-1} \left[h^{(p-1)}(\xi) \sum_{n=1}^{N} k_n^{m-1-p} A_n \right], \; m = 1, \ldots, N. \tag{A.7}$$

For $m = 1$ the right sum above is understood to vanish. The right-hand side is a linear combination of derivatives of h and f. The coefficient matrix of I_n in the left-hand side is the $N \times N$ Vandermonde matrix evaluated at the roots:

$$[V_{mn}] = [k_n^{m-1}] = \begin{bmatrix} 1 & 1 & \cdots & 1 \\ k_1 & k_2 & \cdots & k_N \\ k_1^2 & k_2^2 & \cdots & k_N^2 \\ \vdots & \vdots & \ddots & \vdots \\ k_1^{N-1} & k_2^{N-1} & \cdots & k_N^{N-1} \end{bmatrix}. \tag{A.8}$$

Whenever all roots are distinct this matrix is invertible. Solving (A.7) for I_n yields expressions of the form

$$I_n = L_n[h] - \tilde{L}_n[f], \quad n = 1, \ldots, N, \tag{A.9}$$

where L_n and $\tilde{L}_n$ ($n = 1, \ldots, N$) are linear differential operators of order $N-2$ and $N-1$, respectively, with constant coefficients depending on k_m and A_m. Differentiate the last of (A.7) ($m = N$) once more and use (A.6) to eliminate I_n' to find

$$\sum_{n=1}^{N} k_n^{N} I_n(\xi) = f^{(N)}(\xi) - \sum_{p=1}^{N} \left[h^{(p-1)}(\xi) \sum_{n=1}^{N} k_n^{N-p} A_n \right]. \tag{A.10}$$

Substitute (A.9) into (A.10), collect terms with h and its derivatives on the left, f and its derivatives on the right to arrive at an equation of the form

$$L[h] = G[f], \tag{A.11}$$

where L is a linear differential operator of order at most $N-1$ and G is a linear differential operator of order N, both with constant coefficients depending on k_m and A_m (shown

explicitly in (A.23) and (A.24) below). Thus any solution h of (A.5) satisfies the ODE (A.11) of order $N-1$. Next note from (A.4) that

$$\begin{aligned} I_n(-z) =& 0, \quad n = 1, \ldots, M, \\ I_n(z) =& 0, \quad n = M+1, \ldots, N. \end{aligned} \tag{A.12}$$

Together with (A.9) this yields N boundary conditions for h:

$$\begin{aligned} L_n[h](-z) =& \tilde{L}_n[f](-z), \quad n = 1, \ldots, M, \\ L_n[h](z) =& \tilde{L}_n[f](z), \quad n = M+1, \ldots, N. \end{aligned} \tag{A.13}$$

These are of order $N-2$ for h (shown explicitly in (A.25) below). Hence any solution h of (A.5) necessarily satisfies ODE (A.11) with boundary conditions (A.13). Conversely, let h satisfy (A.11), (A.13). Define I_n by (A.9). Then they satisfy (A.7), (A.10) and (A.12). Differentiate (A.7) and subtract from it (A.7) with m replaced by $m+1$ (subtract (A.10) if $m = N$) to find after some calculation

$$\sum_{n=1}^{N} k_n^{m-1} \left[I_n'(\xi) - k_n I_n(\xi) - A_n h(\xi) \right] = 0, \quad m = 1, \ldots, N.$$

This is a homogeneous linear system for the terms in brackets, whose coefficient matrix is the invertible Vandermonde matrix. Hence the term in brackets above must vanish for each m, therefore (A.6) holds. The unique solution of the IVP (A.6), (A.12) for $I_n(\xi)$ with h given is (A.4). But since I_n satisfies (A.9), setting $m = 1$ in the latter yields (A.5). *We have shown that $h \in C^{N-1}(-z, z)$ is a solution of* (A.5) *if and only if it satisfies the 2-point BVP* (A.11), (A.13).

Observe that the ODE is of order *at most* $N-1$ for h, but there are N boundary conditions. Consider the eigenvalue problem of replacing $f(\xi)$ with $\gamma h(\xi)$ in (A.5), (A.11), (A.13). Recalling that G is an N^{th} order operator, we obtain an N^{th} order ODE for h, $L[h] - \gamma G[h] = 0$ with N boundary conditions of order $N-1$ and the difficulty is removed. Note that in this ODE γ multiplies the highest (N^{th}) derivative of h, so the limit as $\gamma \to 0$ is to be taken with care. The N constants of the general solution of $L[h] - \gamma G[h] = 0$ now satisfy N homogeneous linear equations (from (A.13)) which only have the trivial solution unless the determinant of the coefficient matrix vanishes, which is an algebraic equation of the form $\psi(\gamma, z) = 0$ (the constants are then nonunique unless the normalization condition (17) is enforced.)

Presumably $\psi(\gamma, z) = 0$ can be solved for γ in terms of z. We showed in Section 4 for a piecewise linear kernel, that as $\gamma \to 0$ and z approaches a positive value z_0, such that $\psi(0, z_0) = 0$, h, which is a combination of real exponentials, tends to two delta functions

at $\pm z$. Assuming that this also occurs here, suppose that the solution to the homogeneous integral equation

$$\sum_{n=1}^{N} I_n(\xi) = 0, \quad |\xi| < z \tag{A.14}$$

is of the form

$$h(s) = \alpha_+ \delta(s+z) + \alpha_- \delta(s-z) + h_0(s), \quad |\xi| < z, \tag{A.15}$$

where δ is a delta function and h_0 is suffieciently smooth. For the piecewise quadratic kernel considered in Section 4 , h_0 is a constant. Here $\alpha_\pm$ are unknown constants while the normalization condition (17) becomes

$$\int_{-z}^{z} h_0(s) ds = 1 - \alpha_+ - \alpha_-. \tag{A.16}$$

In view of (A.15) h_0 in place of h in (A.5) solves the integral equation

$$\sum_{n=1}^{N} I_n(\xi) = -\alpha_+ \sum_{n=1}^{M} A_n e^{k_n(\xi+z)} - \alpha_- \sum_{n=M+1}^{N} (-A_n) e^{k_n(\xi-z)}, \quad |\xi| < z. \tag{A.17}$$

Suppose S_j, $j = 0, \ldots, N$, is the j^{th} elementary symmetric function of $\underline{k} = (k_1, \ldots, k_n) \in \mathrm{R}^{\mathrm{N}}$ ($S_0 = 1$, $S_1 = \sum_{n=1}^{N} k_n$, ... , $S_N = \prod_{n=1}^{N} k_n$). Namely, S_j are the fundamental scalar invariants of the diagonal $N \times N$ matrix $\mathrm{diag}(\underline{\mathrm{k}})$ with diagonal entries k_i. Then its characteristic polynomial is

$$P(x) = \det\left(x\mathbf{I} - \mathrm{diag}(\underline{\mathrm{k}})\right) = \prod_{n=1}^{N}(x - k_n) = \sum_{n=0}^{N}(-1)^{N-n} S_{N-n} x^n, \quad x \in \mathbb{R}, \tag{A.18}$$

where $\mathbf{I}$ is the $N \times N$ identity matrix. Let $K = N - 1$ and

$$\underline{k}_{/i} = (k_1, \ldots, k_{i-1}, k_{i+1}, \ldots, k_n) \in \mathrm{R}^{\mathrm{K}}$$

(obtained by removing k_i from $\underline{k}$). The characteristic polynomial of the $K \times K$ matrix $\mathrm{diag}(\underline{\mathrm{k}}_{/\mathrm{i}})$ is

$$P_i(x) = \frac{P(x)}{(x - k_i)} = \det\left(x\mathbf{I} - \mathrm{diag}(\underline{k}_{/i})\right) = \sum_{n=0}^{K}(-1)^{K-n} S_{(K-n,i)} x^n, \ x \in \mathbb{R}.$$

Here $S_{(j,i)}$ is the j^{th} elementary symmetric function of $\underline{k}_{/i}$ with $S_{(0,i)} = 1$ and $\mathbf{I}$ is the $K \times K$ identity matrix. Then the inverse of the Vandermonde matrix (4) has components [6]

$$W_{ij} = \frac{(-1)^{N-j} S_{(N-j,i)}}{P_i(k_i)}. \tag{A.19}$$

In particular, letting the i^{th} Lagrange polynomial be $l_i(x) = P_i(x)/P_i(k_i)$, W_{ij} equals the coefficient of x^{j-1} in $l_i(x)$:

$$l_i(x) = \sum_{j=1}^{N} W_{ij} x^{j-1} = \frac{P_i(x)}{P_i(k_i)}. \tag{A.20}$$

It can be shown that

$$\sum_{i=1}^{N} \frac{k_i^N S_{(N-m,i)}}{P_i(k_i)} = S_{N+1-m}, \quad m = 1, \ldots, N.$$

From this and (A.19) it follows that the solution J_n of $\sum_{n=1}^{N} k_n^{m-1} J_n = d_m$ satisfies

$$\sum_{n=1}^{N} k_n^N J_n = \sum_{m=1}^{N} (-1)^{N-m} S_{N+1-m} d_m. \tag{A.21}$$

Next we write the differential operators in (A.11), (A.13) more explicitly. Letting d_m equal the right-hand side of (A.7), and letting

$$v_0 = 0, \quad v_q = \sum_{n=1}^{N} k_n^{q-1} A_n, \quad q = 1, \ldots N, \tag{A.22}$$

substitute into (A.21) with $m = p + 1$ and subtract the result from (A.10) to find

$$\sum_{p=0}^{N} (-1)^{N-p} S_{N-p} \left[f^{(p)}(\xi) - \sum_{n=0}^{p-1} v_{p-n} h^{(n)}(\xi) \right] = 0, \tag{A.23}$$

or

$$\sum_{p=0}^{N} (-1)^{N-p} S_{N-p} \sum_{n=0}^{p-1} v_{p-n} h^{(n)}(\xi) = \sum_{p=0}^{N} (-1)^{N-p} S_{N-p} f^{(p)}(\xi). \tag{A.24}$$

The above is the explicit form of the differential equation (A.11). Observe that it is of order $N - 1$ in h but order N in f.

Next we express the boundary conditions explicitly. Recall that the solution J_i of $\sum_{n=1}^{N} k_j^{i-1} J_j = d_i$ is $J_i = \sum_{j=1}^{N} W_{ij} d_j$ with W_{ij} as in (17). The boundary conditions (A.12) become, with $K = N - 1$,

$$\begin{aligned}
&\sum_{p=0}^{K} (-1)^{K-p} S_{(K-p,i)} \left[\sum_{n=0}^{p-1} v_{p-n} h^{(n)}(-z) - f^{(p)}(-z) \right] = 0, \quad i = 1, \ldots, M, \\
&\sum_{p=0}^{K} (-1)^{K-p} S_{(K-p,i)} \left[\sum_{n=0}^{p-1} v_{p-n} h^{(n)}(z) - f^{(p)}(z) \right] = 0, \quad i = M+1, \ldots, N.
\end{aligned} \tag{A.25}$$

We now consider the symmetries of the root sets $M^{\pm}(V)$, $N^{\pm}(V)$ in (11) and (13). Let $M_c^{\pm}(V) = M^{\pm}(V) - N^{\pm}(V)$. Then (recall $k_n = i\kappa_n$) $\kappa \in M_c^{+}(V)$ if and only if $-\kappa \in M_c^{-}(V)$. Also $\kappa \in M_c^{\pm}(V)$ if and only if $-\overline{\kappa} \in M_c^{\pm}(V)$, respectively. In addition $\kappa \in N^{\pm}(V)$ if and only if $-\kappa \in N^{\pm}(V)$, respectively. Suppose we keep these symmetries in the truncated set of roots. Hence for some integers $R_{\pm}$, C we will have: $M = 2R_{+}+2C+1$ is the number of roots in $M^{+}(V)$, $N-M = 2R_{-}+2C+1$ is the number of roots in $M^{-}(V)$. Here $R_{\pm}$ is the number of real positive roots in $N^{\pm}(V)$, respectively; C is the number of complex roots in the first quadrant and there is one purely imaginary root in each of $M^{\pm}(V)$; see [9] for details. Recall that $q_{\pm}(\xi)$ and their even derivatives are equal at $\xi = 0$. This implies that all odd coefficients v_m in (A.22) vanish:

$$v_{2q+1} = \sum_{n=1}^{N} k_n^{2q} A_n = 0, \quad q = 0, 1, \ldots \tag{A.26}$$

In particular, $\sum_{n=1}^{N} A_n = 0$ and the coefficient of the highest order derivative $h^{(N-1)}$ in (A.23),(A.24) and $h^{(N-2)}$ in (A.25) vanishes. Hence ODE (A.24) is of order $N-2$ in h and BC (A.25) of order $N-3$ (but still of order N and $N-1$, respectively, in f). This is important. The general solution of the ODE will have $N-2$ undetermined constants, which together with $\alpha_{\pm}$ in (A.15) and z comprise $N+1$ constants. These are to satisfy the $N+1$ conditions (A.25), (A.16).

We turn to the problem for the regular part h_0 of h; see (A.15) through (A.17). Letting $D^n f = f^{(n)}$, the right hand side of (A.11) or (A.24) above is $G[f] = P(D)[f]$ where P is the polynomial in (A.18).Observe that for f equal to the right-hand side of (A.17), $G[f] \equiv 0$ since $P(k_n) = 0$. Hence (A.24) becomes *homogeneous*:

$$\sum_{p=0}^{N} (-1)^{N-p} S_{N-p} \sum_{n=0}^{p-2} v_{p-n} h_0^{(n)}(\xi) = 0, \quad -z < \xi < z. \tag{A.27}$$

The boundary conditions do not; however in the i^{th} equation of (A.25) the term involving f is $P_i(D)[f]$ (see (A); here D is the derivative operator). Note that $P_i(k_j) = 0$ if $i \neq j$, hence we obtain (with $K = N-1$):

$$\begin{aligned}
&\sum_{p=0}^{K} (-1)^{K-p} S_{(K-p,i)} \sum_{n=0}^{p-2} v_{p-n} h_0^{(n)}(-z) = -\alpha_{+} A_i P_i(k_i), \quad i = 1, \ldots, M, \\
&\sum_{p=0}^{K} (-1)^{K-p} S_{(K-p,i)} \sum_{n=0}^{p-2} v_{p-n} h_0^{(n)}(z) = -\alpha_{-}(-A_i) P_i(k_i), \quad i = M+1, \ldots, N.
\end{aligned} \tag{A.28}$$

In (A.27), (A.28) the summation over n has upper limit $p-2$ in view of (A.26). It is understood that the sum is zero for $p < 2$.

The N conditions (A.28) comprise a homogeneous system for the $N-2$ coefficients of the general solution h_0 of (A.27) together with $\alpha^{\pm}$. For nontrivial solutions a determinant involving z has to vanish; this determines z. The resulting loss of uniqueness in the solution of the system is hopefully removed by the additional equation (A.16).

References

[1] W. Atkinson and N. Cabrera. Motion of a Frenkel-Kontorova dislocation in a one-dimensional crystal. *Phys. Rev. A*, 138(3):763–766, 1965.

[2] A. Carpio. Nonlinear stability of oscillatory wave fronts in chains of coupled oscillators. *Phys. Rev. E*, 69:046601, 2004.

[3] A. Carpio and L. L. Bonilla. Oscillatory wave fronts in chains of coupled nonlinear oscillators. *Phys. Rev. E*, 67:056621, 2003.

[4] V. Celli and N. Flytzanis. Motion of a screw dislocation in a crystal. *J. Appl. Phys.*, 41(11):4443–4447, 1970.

[5] Y. Y. Earmme and J. H. Weiner. Dislocation dynamics in the modified Frenkel-Kontorova model. *J. Appl. Phys.*, 48(8):3317–3341, 1977.

[6] M. E.A. El-Mikkawy. Explicit inverse of a generalized Vandermonde matrix. *Applied Mathematics and Computation*, 146(2-3):643 – 651, 2003.

[7] N. Flytzanis, S. Crowley, and V. Celli. High velocity dislocation motion and interatomic force law. *J. Phys. Chem. Solids*, 38:539–552, 1977.

[8] S. Ishioka. Uniform motion of a screw dislocation in a lattice. *Journal of the Physical Society of Japan*, 30(2):323–327, 1971.

[9] O. Kresse and L. Truskinovsky. Mobility of lattice defects: discrete and continuum approaches. *J. Mech. Phys. Solids*, 51:1305–1332, 2003.

[10] V. Nosenko, G. E. Morfill, and P. Rosakis. Direct experimental measurement of the speed-stress relation for dislocations in a plasma crystal. *Phys. Rev. Lett.*, 106(15):155002–155006, 2011.

[11] M. Peyrard and M. D. Kruskal. Kink dynamics in the highly discrete sine-Gordon system. *Physica D*, 14:88–102, 1984.

[12] A. D. Polyanin and A. V. Manzhirov. *Handbook of Integral Equations*. Chapman and Hall/CRC, New York, 2008.

[13] L. A. Sakhnovich. Equations with a difference kernel on a finite interval. *Russian Math Surveys*, 35(4):81–152, 1980.

[14] L. I. Slepyan. *Models and phenomena in Fracture Mechanics*. Springer-Verlag, New York, 2002.

[15] A. Vainchtein. Effect of nonlinearity on the steady motion of a twinning dislocation. *Physica D*, 239:1170–1179, 2010.

[16] A. Vainchtein. The role of spinodal region in the kinetics of lattice phase transitions. *J. Mech. Phys. Solids*, 58(2):227–240, 2010.

[17] J. H. Weiner and W. T. Sanders. Peierls stress and creep in a linear chain. *Phys. Rev.*, 134(4A):1007–1015, 1964.